Static Characteristics of the Qing Dynasty 'Five-tier Outer Eave Column-head Dougong': A Finite Element Simulation Investigation

Lihong Yao,[a] Yuanhe Li,[b] Tongyang Zhou,[b] Dongnan Han,[b] Na Yang,[b,*] and Lijun Liu,[c]

This study systematically investigates the mechanical properties of the Qing Dynasty *"Five-tier Outer Eave Column-head Dougong"* from the Qufu Confucius Temple using finite element numerical simulation. An ANSYS finite element model was established based on orthotropic material properties representative of *Pinus sylvestris* timber, obtained from standardized mechanical tests, incorporating the Hill yield criterion to characterize the plastic development behavior of timber. Through application of vertical monotonic loads and horizontal low-cycle reciprocating loads, the results demonstrate: The vertical ultimate bearing capacity of the dougong reaches 350 kN with a maximum stress value of 21.5 MPa; under horizontal loading. The structure exhibits symmetric hysteretic curve characteristics, with ultimate lateral load-bearing capacities along the X- and Y-principal axes reaching 813 kN and 866 kN, respectively. Numerical analysis yields Y-direction ductility coefficients of 2.58, X-direction ductility coefficients of 3.44, and equivalent viscous damping ratios of 0.103 and 0.111, respectively. Under vertical loading, the mechanical behavior of the structure displays a trilinear stiffness degradation pattern, while under horizontal loading, its mechanical response conforms to a multilinear constitutive model. These findings validate the applicability of finite element numerical simulation in studying the mechanical properties of traditional dougong brackets, providing valuable references, and cost-effective technical means for the conservation and restoration of historical timber structures.

DOI: 10.15376/biores.21.2.5389-5406

Keywords: Dougong bracket; Qing dynasty dougong; Static characteristics; Finite element simulation; Pinus sylvestris

Contact information: a: School of Material Science and Art Design, Inner Mongolia Agricultural University, Hohhot 010018, P.R. China; b: School of Architecture and Art Design, Inner Mongolia University of Science & Technology, Baotou 014010, P.R. China; c: Inner Mongolia Zhongyu Aerospace Engineering Planning and Design Co., Ltd., Baotou 014010, P.R. China;
**Corresponding author: yangnatao@126.com; Lihong Yao and Yuanhe Li contributed equally to this work.*

INTRODUCTION

Confucius Temple No. 7 Pavilion (Fig. 1), Located in Qufu City, Shandong Province (a national key cultural relics protection unit), was built in the 13th year of Qianlong (1749). It is one of the thirteen stele pavilions of the Confucius Temple. Its design and construction strictly adhere to the stipulations of the Qing Dynasty's "Engineering Practice Regulations," the governing code of that era. Bucket arch of the column head of the Pavilion of the Seventh Stele of Confucius Temple is shown in Fig. 2. For the five-step-ang-qiao-dou arch, from the mouth of the lu-dou, the single-elevated single-warp is turned out, the single-warp single-chuck is turned out, and the double-arch method is adopted.

Fig. 1. Confucius temple no. 7 pavilion

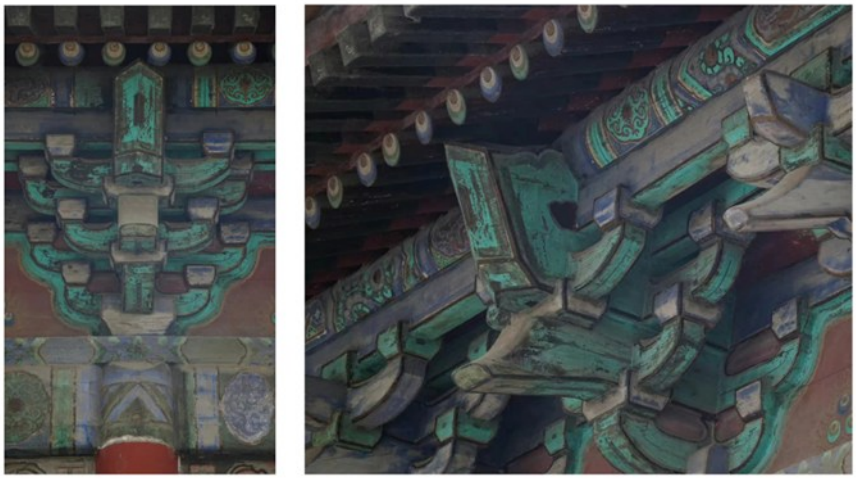

Fig. 2. Confucius temple no. 7 pavilion stele pavilion column head bucket arch

According to the modular system established in the *Yingzao Fashi*, dougong components are categorized into eight grades based on regulatory standards, with each grade equipped with specific dimensional parameters adapted for buildings of different scales (Wu *et al*. 2018; Huan *et al*. 2019; Wang *et al*. 2022). In accordance with the specifications of this Song Dynasty architectural manual, the dougong sample examined in this study falls under the third-grade timber in the cai-fen modular system (Chen *et al*. 2025). The manual explicitly states that the unit value of 1 fen° for third-grade timber is defined as 15.5 mm. Specifically, the research examines the outer eave column-head dougong of Dule Temple Gate, comprising 62 modular units—44 primary members and 18 wooden pins—categorized into load-bearing and connective types. Figure 3 shows a

schematic representation of the experimental model in both full perspective and exploded views, delineating its layered composition.

It should be clarified that the dougong investigated in this study originates from a Qing Dynasty building constructed in 1749. The geometric configuration, member dimensions, and structural relationships of the bracket system are determined based on direct observation and measurement of the existing Qing Dynasty architectural remains at the Confucius Temple in Qufu. Therefore, the mechanical analysis conducted in this research is fundamentally grounded in Qing Dynasty construction practice and material assembly logic, rather than theoretical assumptions derived from earlier dynastic regulations.

In this context, the Yingzao Fashi is referenced only as a historical technical document for terminology clarification and basic dimensional description. It is not used as a regulatory standard for Qing Dynasty architecture. The primary basis for structural interpretation remains the Qing-style dougong configuration derived from the actual architectural specimen, ensuring that the analysis is consistent with Qing Dynasty construction characteristics.

Fig. 3. Structural test model of bucket arch in Qing Dynasty

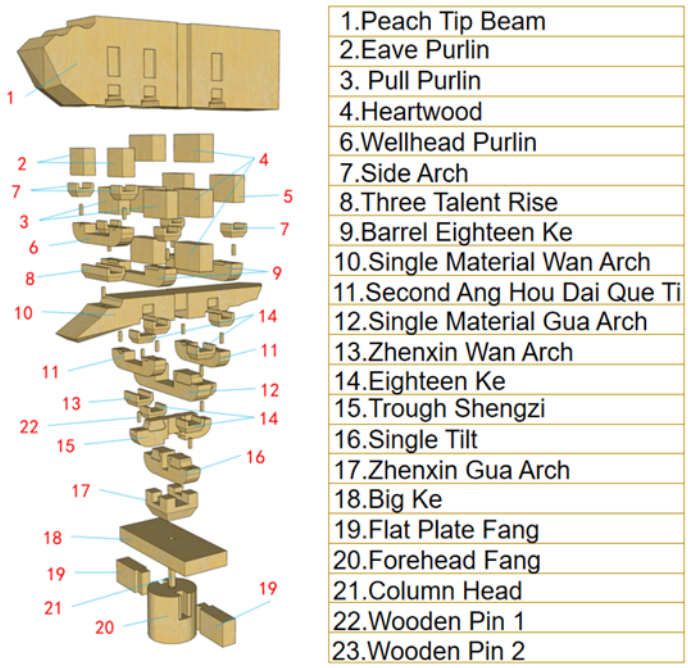

Fig. 4. The exploded assembly diagram of 'Five-tier Outer Eave Column-head Dougong Bracket' test model of the Dule Temple Gate

Economic feasibility constitutes a primary constraint in experimental research on traditional timber structures. The construction of full-scale dougong models, for instance, requires substantial material consumption and labor investment, resulting in particularly pronounced cost pressures (Meng *et al*. 2019; Lu *et al*. 2025). Conventional mechanical testing techniques are constrained by their reliance on instrumented measurement points, where inherent systematic errors and limited spatial resolution reduce the accuracy of measured results in complex structural systems (Fang *et al*. 2001; D'Ayala and Tsai 2008). In contrast, finite element numerical simulation — refined through long-term methodological advancements and empirical validation (Suzuki and Maeno 2006; Wu *et al*. 2020; Cheng *et al*. 2023)—has become an essential computational approach for investigating the mechanical behavior of dougong brackets. This technical shift offers two major advantages: it not only eliminates the financial investment required for physical specimen preparation, but it also enables precise control over boundary conditions and material anisotropy, thereby providing an effective means for targeted mechanical analysis of critical structural regions (D'Arenzo *et al*. 2024).

This study employs high-fidelity finite element modeling to conduct a comprehensive investigation into the static performance of Qing Dynasty Five-tier Outer Eave Column-head Dougong brackets. The computational framework incorporates three fundamental mechanical evaluation criteria: structural load-bearing capacity—including ultimate load levels and stress distribution patterns; deformation response—involving stiffness evolution and displacement field characteristics; and energy dissipation—encompassing hysteretic behavior and damping conversion mechanisms. By accurately simulating vertical (Z-axis) monotonic loading and biaxial (X/Y-axis) cyclic loading protocols, a validated numerical assessment system for historic timber structure performance has been established. This computational methodology maintains strong agreement with experimental data while significantly reducing testing requirements,

providing a scientific basis for digital analysis of traditional construction techniques and the development of conservation strategies.

Previous studies on Qing-style timber structures have shown that Qing Dynasty dougong brackets exhibit stable load-transfer mechanisms and well-defined construction logic, providing an important empirical basis for numerical analysis of their mechanical behavior.

The novelty of this study lies in the integrated mechanical evaluation of a Qing Dynasty five-tier outer eave column-head dougong based on detailed finite element modeling. Unlike previous studies that primarily focused on simplified configurations or individual mechanical indicators, this research systematically examines load-bearing capacity, deformation behavior, stiffness degradation, and stress distribution within a unified analytical framework. By adopting a Qing-style dougong specimen derived from actual architectural remains, this study provides a more comprehensive understanding of the mechanical characteristics of Qing Dynasty bracket systems.

Although Qing Dynasty dougong systems are no longer commonly used in modern construction, their underlying mechanical principles remain relevant to contemporary timber engineering. The complex load-transfer behavior, joint nonlinearity, and energy dissipation mechanisms observed in traditional dougong structures provide valuable insights for the design of modern timber systems, including post-and-beam and CLT-based structures. The present study aims to extract transferable mechanical characteristics from historical dougong assemblies through numerical analysis, thereby informing both heritage conservation and modern timber structural design.

EXPERIMENTAL

Finite Element Simulation

The finite element model developed in this study adopted material properties of *Pinus sylvestris* timber with a moisture content of 12% to represent the mechanical behavior of traditional timber components. The mechanical property parameters adopted in the numerical model were obtained in strict accordance with standardized testing procedures reported in the literature: the air-dry density was measured at 0.493 g/cm³ (GB/T 1933-2009), while key parameters including elastic modulus, Poisson's ratio, and shear modulus were determined using strain sensing technology (GB/T 15777-2017, GB/T 1943-2009, LY/T 3297-2022). Strength test results were as follows: longitudinal compressive strength 35.2 MPa (GB/T 1935-2009), transverse compressive strength 5.14 MPa (GB/T 1939-2009), and flexural strength 52.9 MPa (GB/T 1936.1-2009), with complete data provided in the Appendix, Supplementary Table 1.

This study developed a finite element computational model of the dougong bracket system using the ANSYS Workbench 2021 R1 multi-physics simulation platform. Material constitutive parameters were calibrated through inverse analysis of experimental data, with elastic characteristics modeled using orthotropic constitutive relationships (Yao and Li 2023), while plastic behavior was described by Hill's anisotropic yield criterion. The orthotropic mechanical properties exhibited by timber were fully characterized by nine independent elastic parameters, specifically including: elastic moduli (E_L, E_R, E_T) defining the stiffness along three material principal directions, shear moduli (G_{LR}, G_{LT}, G_{RT}) representing the shear response on three orthogonal planes, and Poisson's ratios (V_{LR}, V_{LT}, V_{RT}) describing the strain coupling relationships between the three directions.

Table 1. Elastic Modulus, Poisson's Ratio, and Shear Modulus of *Pinus sylvestris*

	E_L	E_R	E_T	V_{LR}	V_{LT}	V_{RT}	G_{LR}	G_{LT}	G_{RT}
P. sylvestris	8023	1103	843	0.422	0.513	0.687	652	345	231

The material's elastic moduli are longitudinal E_L, radial E_R, and tangential E_T (MPa). Poisson's ratios V_{LR} and V_{LT} quantify transverse strains induced by longitudinal tension, whereas V_{RT} (μ TR) reflects tangential strain caused by radial stress. The shear moduli are defined as follows: G_{LR} (longitudinal-radial) and G_{LT} (longitudinal-tangential), both in MPa, while G_{RT} denotes the planar (radial-tangential) shear modulus, also in MPa.

Loading Protocol

The experimental loading scheme was designed according to the coordinate system shown in Fig. 5. Monotonic static loading (Wu *et al*. 2024) was applied along the Z-axis to represent permanent load conditions, whereas bidirectional low-cycle reciprocating displacements (An *et al*. 2025; Meng *et al*. 2025) were introduced along the Y- and X-axes to simulate seismic conditions.

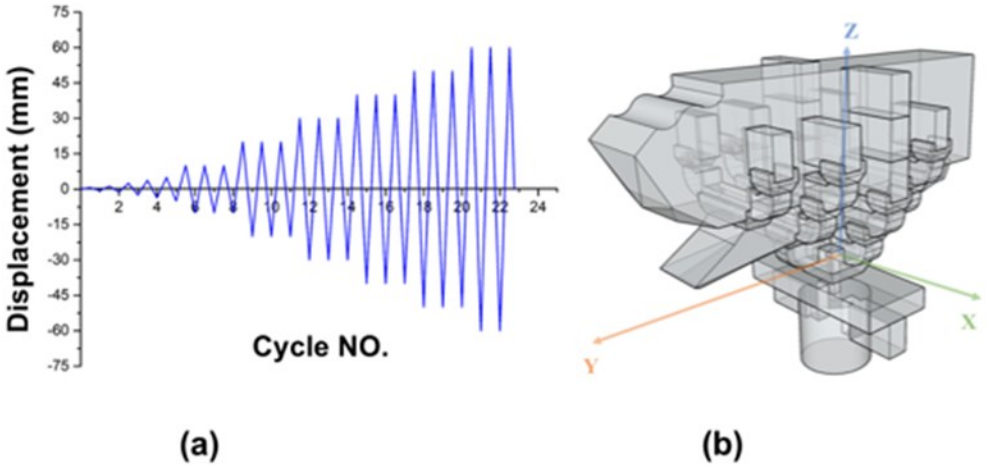

Fig. 5. The loading protocol (a); and direction definition of the test model in the coordinate axis (b)

Based on Niu's (2017) experimental framework, this investigation adopted vertical monotonic static loading to replicate the load transfer characteristics of permanent roof loads in traditional dougong configurations. An initial vertical load of 60 kN, determined through architectural specifications and structural analysis, was implemented. The experimental procedure involved a dual-phase control approach: initial force-controlled loading at 5 kN/min continued until yield identification (characterized by observable deformation or pronounced nonlinearity in the load-displacement response), with subsequent transition to displacement-controlled loading at 2 mm/min for assessment of post-yield mechanical behavior. The test concluded when structural collapse occurred (characterized by a reduction in load capacity to 80% of the maximum resistance) or when extensive damage prevented further loading. This two-phase methodology enabled complete documentation of both elastic and plastic deformation characteristics under controlled conditions throughout the entire failure process.

Displacement-controlled methodology (Yao and Li 2023) was implemented in horizontal low-cycle repeated tests to conduct quasi-static analysis. The loading sequence consisted of two distinct stages: Initial application of five amplitude-progressive cycles

(ranging from 0.0125Δ to 0.1Δ, with Δ = 50 mm), subsequently followed by systematically increasing displacement phases commencing at 0.2Δ with 0.2Δ stepwise progression, each subjected to three full loading cycles (Cao *et al*. 2023). The schematic representation of the loading regime is provided in Fig. 5a. Computational modeling ensured alignment with experimental configurations through accurate reproduction of solver settings, kinematic restrictions, and multi-directional boundary constraints (Z/Y/X axes). Detailed parameter arrangements are presented in Fig. 5b.

The applied displacement is imposed along the vertical Z-axis to simulate vertical loading, while the X- and Y-axes represent the horizontal directions. The displacement direction is consistent throughout the numerical analysis.

Grid System

A hybrid hexahedral-tetrahedral meshing strategy was adopted, implemented with second-order elements. The discretization followed a geometric criterion: Hexahedral elements for regular domains and tetrahedral elements for complex geometries. Figure 6 illustrates the resulting assembled mesh of the dougong bracket.

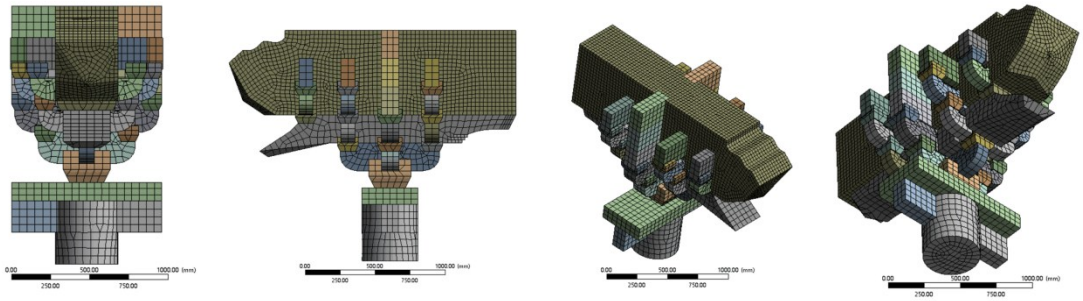

Fig. 6. The grid system of bucket arch in Qing Dynasty

RESULTS AND DISCUSSION

Vertical Monotonic Static Loading (Z-axis)

The load-displacement relationship derived from the vertical (Z-axis) monotonic loading simulation is illustrated in Fig. 7. The curve demonstrates progressive divergence in load-bearing capacity after reaching 350 kN. Von Mises stress analysis (Fig. 8A) identifies principal stress concentrations along the load transfer path in upper structural elements, reaching maximum values of 27.4 MPa at the central mortise-tenon joint of the historic dougong. Corresponding elastic strain patterns (Fig. 8B) show remarkable consistency, with peak values of 0.040 at the same critical connection. A strong correlation exists between the strain energy distribution (Fig. 8C) and regions of stress concentration. The dougong assembly accumulated 83,900 MJ of strain energy, thereby verifying the effectiveness of the vertical load transfer path from upper structures to supporting columns. Measured displacements (Fig. 8D) gradually diminish radially from the maximum value of 136 mm at the Liaoyanfang apex, revealing the characteristic layered deformation mechanism typical of traditional timber constructions subjected to vertical loads.

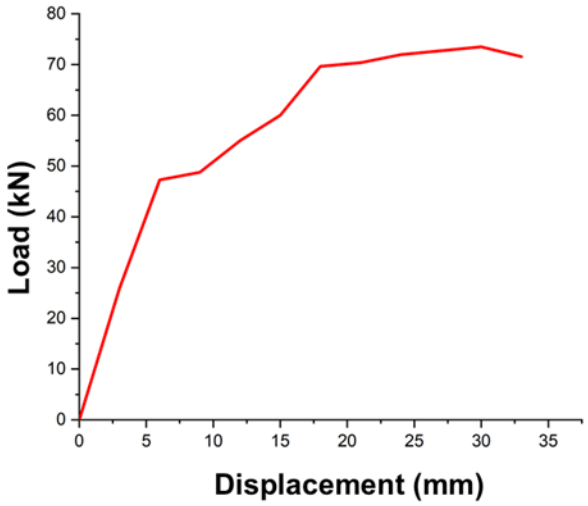

Fig. 7. The load-displacement curve (Z axis) of the Qing Dynasty bucket arch test model

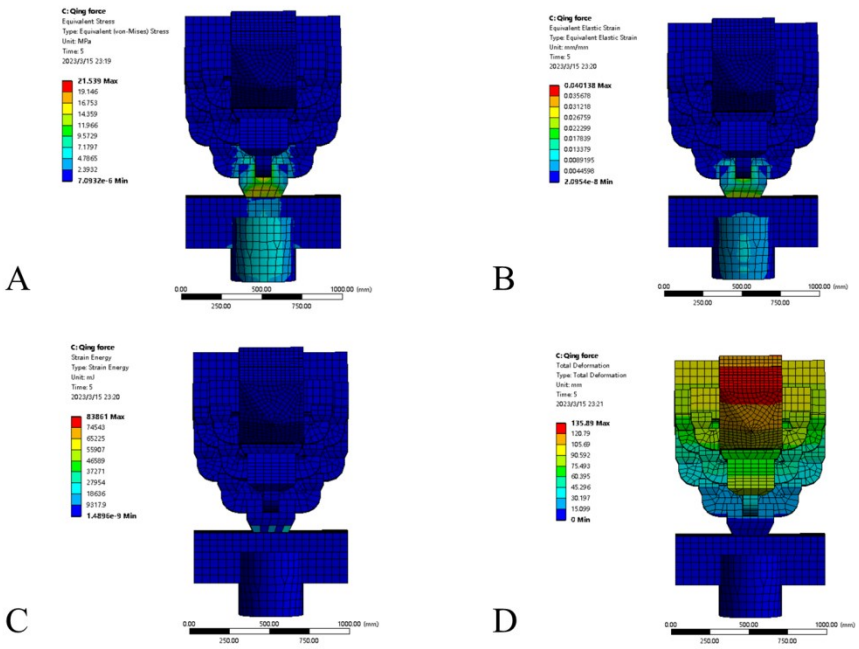

Fig. 8. Equivalent stress (A), equivalent elastic strain (B), strain energy (C), overall deformation nephogram (D) in Z-axis

Horizontal Low-Cycle Reciprocating Loading (Y- and X-axes)

Horizontal low-cycle reciprocating simulations along the Y- and X-axes (Fig. 9) revealed the dougong's hysteresis behavior. The model demonstrated peak lateral loads of 866 kN (Y-axis) and 813 kN (X-axis). The symmetrical, spindle-shaped hysteresis curves observed in both directions confirm the bracket's substantial energy dissipation and stable plastic deformation capacity.

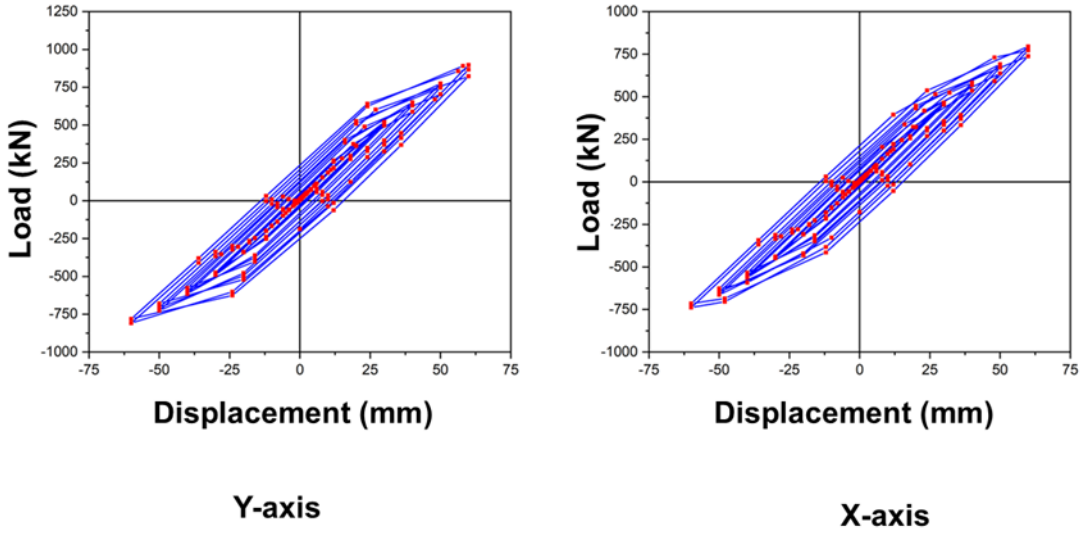

Fig. 9. The load-displacement hysteretic curves in Y- and X-axes

The load-displacement skeleton curve was constructed from the envelope of the hysteretic loops (Fig. 10). From this skeleton curve, the stiffness degradation behavior was quantified by computing the secant stiffness for each loading cycle, with the resulting curve provided in Fig. 11.

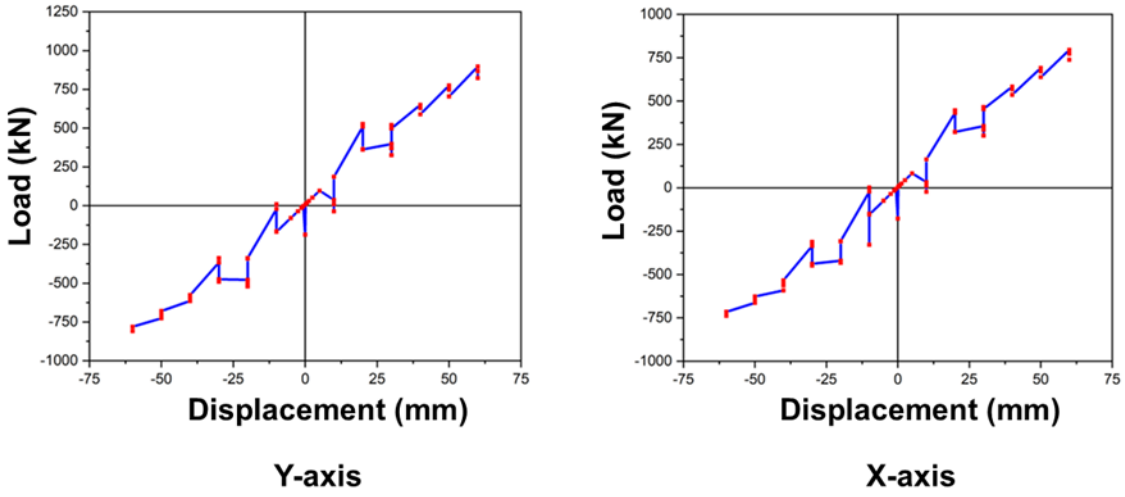

Fig. 10. The skeleton curve of bucket arch in Qing Dynasty on Y- and X-axes (simulation)

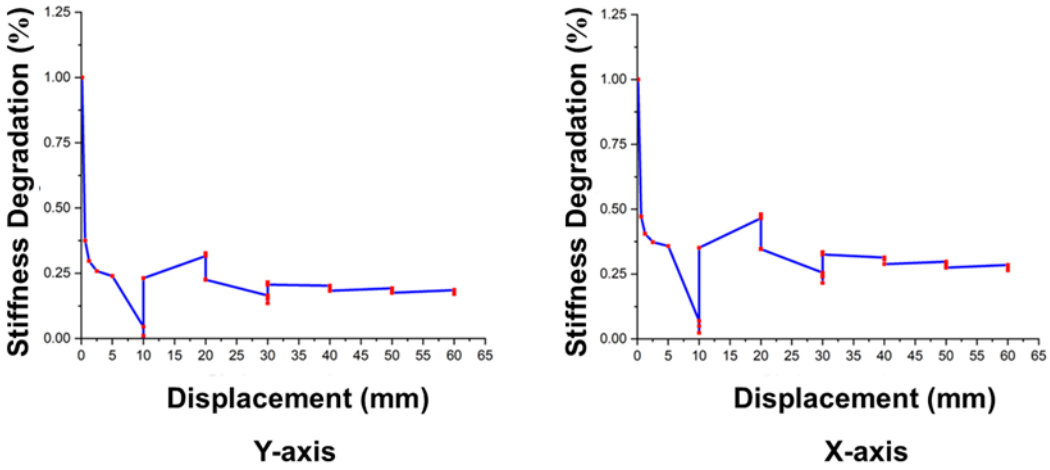

Fig. 11. The stiffness degradation curve of bucket arch in Qing Dynasty on Y- and X-axes (simulation)

The non-smooth stiffness evolution observed in Fig. 11 is primarily associated with contact nonlinearity and slip behavior at the mortise–tenon interfaces.

Significant stress concentration is exhibited at the Qing Dynasty dougong-column head interface, where the von Mises stress peaks at 21.5 MPa in the Huagong-Sandou joint (Fig. 12A). A corresponding pattern is observed in the equivalent elastic strain field (Fig. 12B), with a maximum value of 0.040 at the Dacai-Pingfang node. This localized concentration is corroborated by the strain energy density (Fig. 12C), which reaches 2.41 ×10^6 MJ at the same location, demonstrating spatial alignment with the stress field. The effective transfer of energy within the arch-rafter-bucket structural system is confirmed by this synergistic phenomenon, which also establishes the joint as the key region for energy dissipation. A distinct hierarchical deformation pattern is displayed in the displacement field (Fig. 12D), featuring a peak displacement of 4.71 mm at the Dacai-Pingfang joint that gradually diminishes across subordinate structural elements such as the Taojianliang, Er'ang, Shanqiao, Ludou, and Zhengxin melon arches.

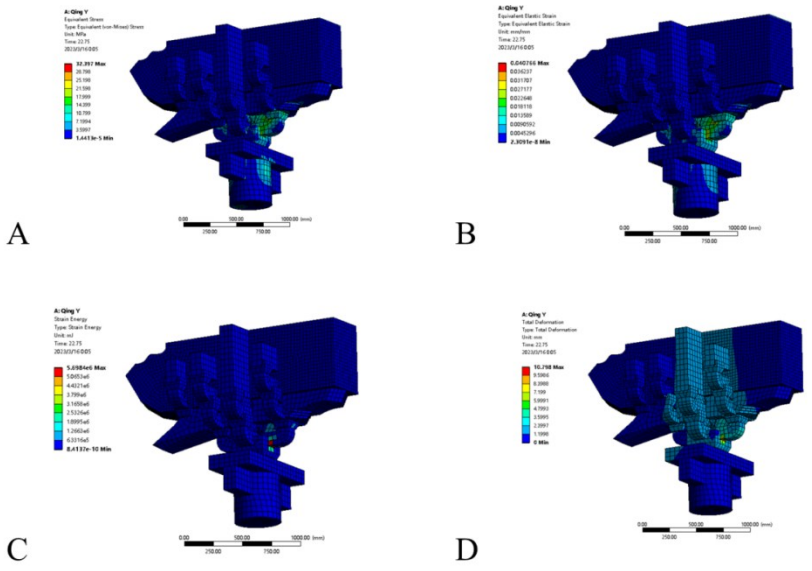

Fig. 12. Nephograms of equivalent stress (A), equivalent elastic strain (B), strain energy density (C), and total deformation under Y-axis loading (D)

As shown in Fig. 12, the maximum strain is predicted to be concentrated at the contact region between the dougong arm and the column-head component, which is primarily associated with local stress concentration under lateral loading. The red region indicates the location of maximum strain, which is concentrated at the contact area between the dougong arm and the column-head component.

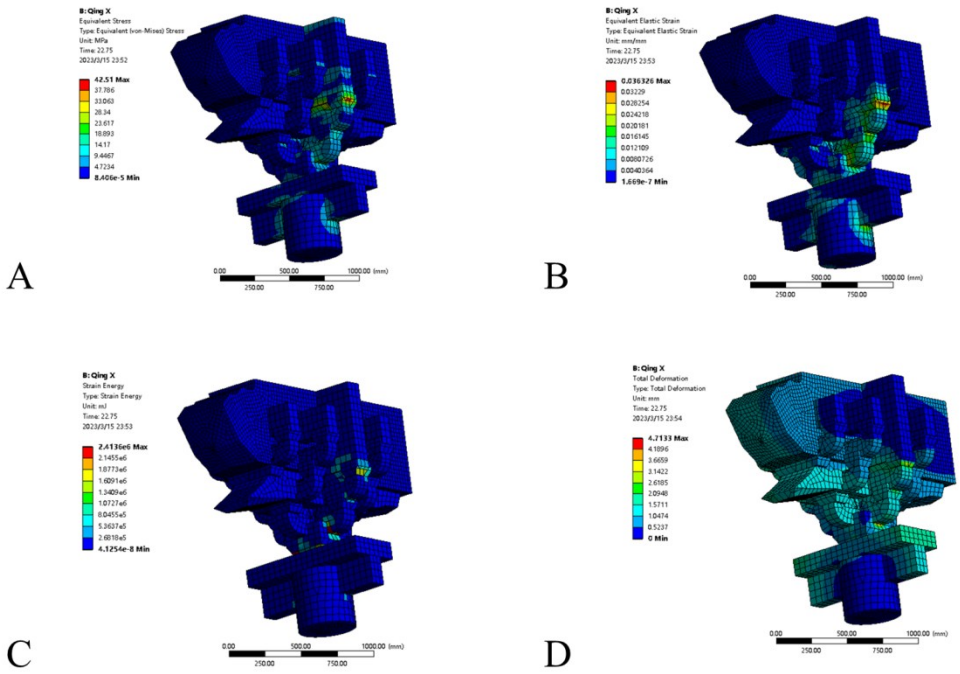

Fig. 13. Equivalent stress (A), equivalent elastic strain (B), strain energy (C), overall deformation nephogram (D)

During quasi-static X-direction loading, the von Mises stress field (Fig. 13A) demonstrates critical concentrations reaching 42.5 MPa, particularly localized at the mortise-tenon connection between the right Mangong and Nidaogong, along with the interfacial region linking the right Nidaogong to the column head. This stress distribution shows spatial correlation with maximum equivalent elastic strain values of 0.036 measured at the right-center melon arch, right-center ten-thousand arch, and slot lifter components (Fig. 13B), verifying field congruence between stress and strain responses. Strain energy density distributions (Fig. 13C) demonstrate geometric correspondence with the stress field, reaching 2.41×10^{6} MJ at the Da Cai-Ping Fang interface. The marked energy accumulation establishes the mortise-tenon joint as the dominant energy dissipation pathway under cyclic loading conditions. Deformation measurements (Fig. 13D) identify peak displacements of 4.71 mm on the right side of the Mangong, with successively decreasing deformation gradients propagating toward the foundation—consistent with established deformation characteristics of historical timber structures subjected to lateral loads.

Comprehensive analysis of stress, strain, and energy distributions identifies the Mangong/San Dou interface as a potential initiation zone for structural failure. This assessment is supported by mechanical stress and strain energy density values exceeding critical thresholds documented in comparable timber joints. The identified failure mechanism aligns with damage patterns historically observed in timber structures subjected to cyclic lateral loading.

Mechanical Model for Static Structural Performance (Z-, Y-, and X-Axes)

Under monotonic Z-axis loading, the dougong demonstrated a triphasic stiffness degradation pattern (Fig. 14). The initial phase OA (0–ΔA) was characterized by reduced stiffness (K_{OA} = 9.63 kN/mm, Eq. 1) arising from contact nonlinearities. Subsequent phase AB (ΔA–ΔB) exhibited consistent stiffness (K_{AB} = 4.37 kN/mm, Eq. 2) following complete engagement of structural components. The final phase BC (ΔB–ΔC) displayed progressive stiffness deterioration (K_{BC} = 2.65 kN/mm, Eq. 3) caused by yielding in mortise-tenon connections and accumulated structural damage.

$$k_{OA} = \frac{P_x}{\Delta_x} \quad (1)$$

$$k_{AB} = \frac{P_y - P_x}{\Delta_y - \Delta_x} \quad (2)$$

$$k_{BC} = \frac{P_b - P_y}{\Delta_b - \Delta_y} \quad (3)$$

In these equations, kOA, kAB, and kBC denote the secant stiffness values corresponding to the OA, AB, and BC segments of the trilinear load–displacement model, respectively. Px, Py, and Pb represent the characteristic load values at points A, B, and C, while Δx, Δ*y*, and Δ*b* denote the corresponding displacements.

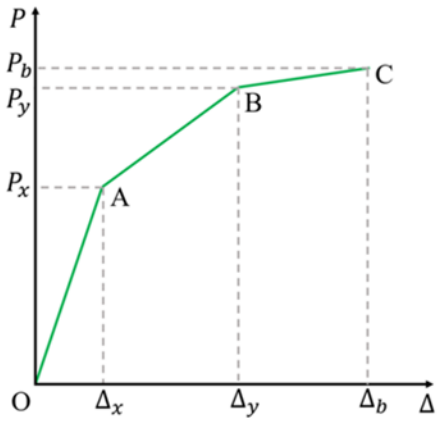

Fig. 14. The static behavior model of bucket arch in Qing Dynasty on Z-axis

Hysteretic and skeleton curve data enable the establishment of a restoring force model (Fig. 15) for the five-tiered outer eave column-head dougong, effectively representing its static structural performance under Y- and X-axes loading conditions.

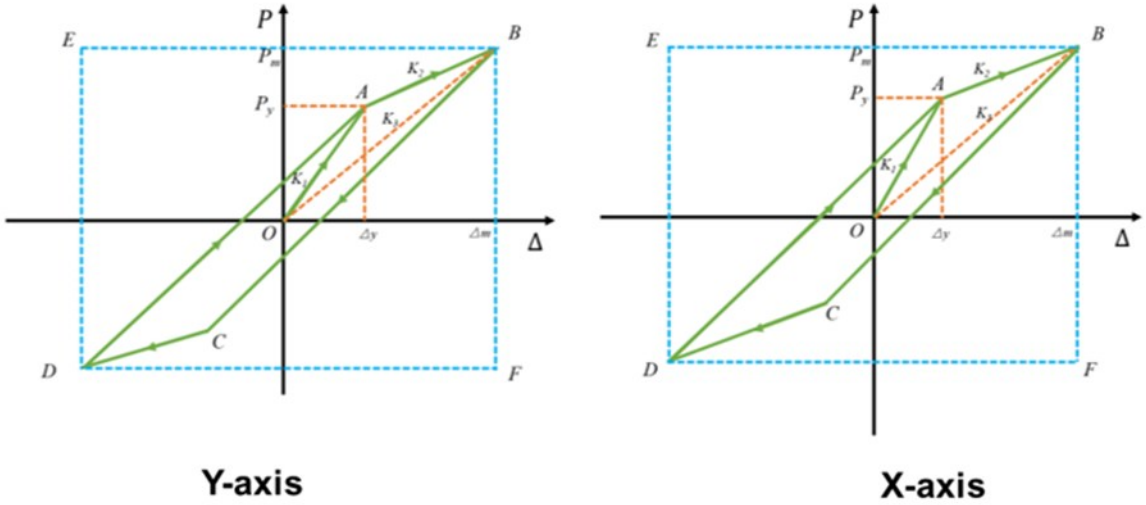

Fig. 15. The static behavior model of bucket arch in Qing Dynasty on Y- and X-axes

The restoring force model along the Y-axis demonstrates three distinct mechanical phases. The initial OA phase represents elastic deformation, where load is proportional to displacement with a primary stiffness (K_{Y1}) of 24.12 kN/mm. Subsequently, the AB phase captures yielding behavior, characterized by a reduced plastic stiffness (K_{Y2}) of 9.74 kN/mm. The effective stiffness (K_{Y3}), defined as the ratio of peak load capacity to maximum displacement in the restoring force model, is determined to be 14.5 kN/mm for the dougong bracket. A similar tri-phasic mechanical response is observed under X-axis loading, with corresponding stiffness values of K_{X1} = 26.7 kN/mm (elastic), K_{X2} = 3.87 kN/mm (plastic), and K_{X3} = 11.7 kN/mm (effective). When the dougong component in historic wooden structures is conceptualized as an anti-seismic damping interface linking the roof and the column-beam system, the energy dissipation capacity can be quantitatively evaluated using the nonlinear parameter NL. Two key seismic performance metrics were evaluated. The nonlinear coefficient (NL), derived from the area ratio of the restoring force model's envelope to the reference rectangle SBDEF (Fig. 15), serves as a metric for energy

dissipation. The obtained NL values are 0.154 (Y-axis) and 0.189 (X-axis). Ductility, defined as the ultimate-to-yield displacement ratio, characterizes deformation ability. The model exhibited ductility coefficients of 2.58 (Y-axis) and 3.44 (X-axis), with the higher X-axis value confirming better deformability in that direction. Here, NL denotes the nonlinear energy dissipation coefficient, defined as the ratio between the enclosed area of the hysteretic envelope and the reference rectangular area in the restoring force model.

Where KY1, KY2, and KY3 represent the elastic stiffness, plastic stiffness, and effective stiffness of the restoring force model along the Y-axis, respectively (kN/mm). Correspondingly, KX1, KX2, and KX3 denote the stiffness parameters along the X-axis.

Energy dissipation performance is directly proportional to the equivalent viscous damping coefficient (h_e), with higher values indicating superior capacity. As determined from Fig. 16 and Eq. 4, the five-tiered outer eave column-head dougong bracket exhibits he values of 0.103 under Y-axis loading and 0.111 under X-axis loading, reflecting its orientation-dependent damping characteristics.

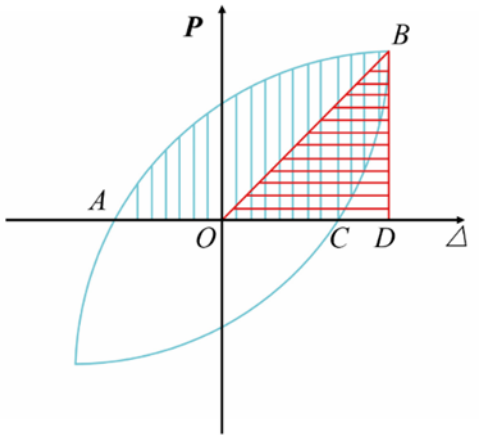

Fig. 16. Calculation of equivalent viscous damping coefficient

$$h_e = \frac{1}{2\pi} \cdot \frac{S_{ABC}}{S_{OBD}} \quad (4)$$

In Eq. 4, h_e denotes the equivalent viscous damping coefficient; S_ABC represents the enclosed area of the hysteretic loop, and S_OBD denotes the area of the reference triangle defined by the peak load and corresponding displacement, as illustrated in Fig. 16.

A comprehensive assessment was conducted to investigate the three-dimensional (X-, Y-, Z-axes) static behavior and stress-strain properties of a five-level exterior eave column-top dougong assembly. Under Z-axis vertical monotonic loading, the structure demonstrated a tri-linear elastic response with multi-phase stiffness degradation. The mechanical behavior sequentially involved: (I) initial compaction of gaps at component interfaces; (II) a stable linear-elastic phase with consistent stiffness; and (III) a final yielding phase culminating in structural failure. The dougong bracket system under bidirectional (Y- and X-axes) low-cycle reciprocating loading demonstrates mechanical response conforming to a multi-linear restoring force pattern, characterized by sequential elastic, yielding, and ultimate failure phases. This process manifests continuous stiffness reduction, while the conspicuous pinching effect evident in hysteresis loops near the origin suggests the presence of interface slippage. Beyond critical loading stages, significant plastic deformation develops concurrently with accelerated displacement growth. As

tabulated in Table 2, principal mechanical parameters—assessed triaxially through strength, deformation, and energy dissipation metrics—confirm that structural failure initiates at critical nodal connections under overload scenarios, leading to system-wide progressive collapse through force.

Although this study is primarily based on finite element simulation, the modeling strategy and material parameters adopted in this research follow established approaches reported in previous experimental and numerical studies on traditional timber structures. The constitutive models, boundary conditions, and loading protocols were defined according to standardized testing data and commonly accepted simulation practices.

Moreover, the mechanical response characteristics obtained in this study, including load–displacement behavior, stiffness degradation, and stress concentration patterns, are consistent with those reported in comparable investigations of traditional dougong and timber bracket systems. These consistencies indicate that the adopted numerical simulation approach is capable of capturing the essential mechanical behavior of the investigated Qing Dynasty dougong structure.

Previous numerical studies on traditional dougong systems, such as those focusing on early dynastic structures exemplified by the Tang Dynasty Nanchan Temple, have provided valuable insights into the mechanical behavior of bracket systems under specific loading conditions. These studies typically emphasized simplified structural configurations or individual response indicators.

In contrast, the present study focuses on a Qing Dynasty five-tier outer eave column-head dougong derived from actual architectural remains and adopts an integrated mechanical evaluation framework. By simultaneously examining load-bearing capacity, deformation behavior, stiffness degradation, and stress distribution, this study extends existing research by providing a more comprehensive assessment of the mechanical characteristics of Qing Dynasty dougong systems.

Table 2. Characteristic Values of the Six Specimen Configurations

Name	The Key Mechanical Indexes of Bucket Arch in Qing Dynasty						
Pathway	Numerical Simulation						
Intensity		Deformation			Energy Dissipation		
F_{Z1}	F_{Z2}	K_{Z1}	K_{Z2}	K_{Z3}	NL(Y)		
307.23	349.66	9.63	4.37	2.65	0.154		
F_{Y1}	F_{Y2}	K_{Y1}	K_{Y2}	K_{Y3}	NL(X)		
866.43	866.43	24.12	9.74	14.48	0.189		
F_{X1}	F_{X2}	K_{X1}	K_{X2}	K_{X3}	H_Y		
812.58	812.58	26.66	3.87	11.72	0.103		
		U_Y	U_X		H_X		
		2.58	3.44		0.111		

The structural performance is characterized by a comprehensive parameter system. Along the Z-axis, bearing capacity is quantified through yield (F_{Z1}) and ultimate (F_{Z2}) values in kN, while stiffness progression is described by initial (K_{Z1}), yield (K_{Z2}), and ultimate (K_{Z3}) phases in kN/mm. For horizontal loading, maximum thrust capacities are defined by F_{Y1}-F_{Y2} (Y-axis) and F_{X1}-F_{X2} (X-axis) in kN. Corresponding stiffness parameters include elastic (K_{Y1}, K_{X1}), plastic (K_{Y2}, K_{X2}), and effective values (K_{Y3}, K_{X3}) in kN/mm. Additional performance metrics comprise ductility (UY, UX), nonlinear coefficients (NL(Y), NL(X)), and equivalent viscous damping coefficients (HY, HX) for both horizontal directions.

CONCLUSIONS

It should be noted that the reported numerical values represent approximate estimates derived from numerical simulation based on adopted material properties, which are subject to inherent uncertainty associated with timber variability.

1. The Qing Dynasty dougong's mechanical behavior is well captured by a variable-stiffness linear elastic model when subjected to Z-axis monotonic loads, whereas its hysteretic response under bidirectional (X- and Y-axes) low-cycle reciprocating loads is effectively represented through a restoring force model.
2. The Qing Dynasty dougong bracket exhibited the following approximate strength-level capacities: a yield bearing capacity of about 307 kN and an ultimate bearing capacity of approximately 350 kN under Z-axis loading, a maximum horizontal thrust of about 866 kN along the Y-axis, and a peak forward thrust of approximately 813 kN along the X-axis.
3. Deformation-level analysis of the Qing Dynasty dougong bracket revealed the following stiffness properties: Z-axis values of 9.63 kN/mm (initial), 4.37 kN/mm (yield), and 2.65 kN/mm (deformation); Y-axis parameters of 24.1 kN/mm (elastic), 9.74 kN/mm (plastic), 14.5 kN/mm (effective) with 2.58 ductility; X-axis values of 26.7 kN/mm (elastic), 3.87 kN/mm (plastic), and 11.7 kN/mm (effective) with 3.44 ductility.
4. Energy-dissipation evaluation of the Qing Dynasty dougong bracket yielded the following parameters: Y-axis measurements showed a nonlinear coefficient of 0.154 with an equivalent viscous damping coefficient of 0.103, while X-axis values registered 0.189 and 0.111 respectively.
5. The finite element analysis corroborated the structural wisdom of the dougong bracket, with key mechanical indices (including an ultimate bearing capacity of 349.66 kN and a ductility coefficient of 3.44) confirming that Qing Dynasty builders achieved a sophisticated balance between efficient load transfer and inherent seismic resilience.

ACKNOWLEDGMENTS

This work was supported by the National Natural Science Foundation of China-Regional Science Foundation Project 'Construction of Static Structural Performance Evaluation System for *Five-tier Outer Eave Column-head Dougong Bracket* Components' (32360356), with additional support from the Scientific Research Projects of First-class Disciplines (Grant No. YLXKZX-NKD-027) and Scientific research support of Inner Mongolia University of Science & Technology (Grant No. KJJH2023948).

The authors used DeepSeek artificial to polish the text. The images, numbers, graphics, or diagrams in this article are not produced using any generative AI.

REFERENCES CITED

An, R., Yuan, J., Pan, Y., and You, W. (2025). "Experimental and parametric study on rotational performance of through-tenon joints in traditional timber structures," *International Journal of Architectural Heritage* 19(3), 293-312. https://doi.org/10.1080/15583058.2023.2284745

Cao, J., Li, X., Liu, Y., Qian, H., and Yu, D. (2023). "Seismic performance investigation of the Dou-gong joints of traditional Chinese timber structures," *European Journal of Wood and Wood Products* 81(1), 173-186. https://doi.org/10.1007/S00107-022-01863-X

Chen, C., Li, Y., Han, D., Kang, H., and Li, Y. (2025). "Simulation study on the static characteristics of 'Five-tier Outer Eave Column-head Dougong Bracket' from the main hall of Nanchan Temple in Tang Dynasty," *BioResources* 20(3), 6082-6099. https://doi.org/10.15376/biores.20.3.6082-6099

Cheng, Y., He, H., Sun, H., and Cheng, S. (2023). "Experimental study and mechanism analysis of out-of-plane seismic performance of reinforced concrete shear walls," *Journal of Building Engineering* 80, article 108058. https://doi.org/10.1016/j.jobe.2023.108058

D'Arenzo, G., Ruggeri, E. M., and Fossetti, M. (2024). "Lateral performance of cross-laminated timber shear walls connected to perpendicular walls: Experimental tests and analytical modeling," *Journal of Structural Engineering* 150(8), article 04024080. https://doi.org/10.1061/JSENDH.STENG-13151

D'Ayala, D. F., and Tsai, P. H. (2008). "Seismic vulnerability of historic Dieh–Dou timber structures in Taiwan," *Engineering Structures* 30, 2101-2113. https://doi.org/10.1016/j.engstruct.2007.11.007

Fang, D. P., Iwasaki, S., Yu, M. H., Shen, Q. P., Miyamoto, Y., and Hikosaka, H. (2001). "Ancient Chinese timber architecture. II: Dynamic characteristics," *Journal of Structural Engineering* 127(11), 1358-1364. https://doi.org/10.1061/(ASCE)0733-9445(2001)127:11(1358)

GB/T 15777 (2017). "Method for determination of the modulus of elasticity in compression parallel to grain of wood," Standardization Administration of China, Beijing, China.

GB/T 1933 (2009). "Method for determination of the density of wood," Standardization Administration of China, Beijing, China.

GB/T 1935 (2009). "Method of testing in compressive strength parallel to grain of wood," Standardization Administration of China, Beijing, China.

GB/T 1936.1 (2009). "Method of testing in bending strength of wood," Standardization Administration of China, Beijing, China.

GB/T 1939 (2009). "Method of testing in compression perpendicular to grain of wood," Standardization Administration of China, Beijing, China.

GB/T 1943 (2009). "Method for determination of the modulus of elasticity in compression perpendicular to grain of wood," Standardization Administration of China, Beijing, China.

Huan, J., Ma, D., Wang, W., and Wang, Z. (2019). "Safety state evaluation method based on attribute recognition model for ancient timber buildings," *Advances in Civil Engineering* 2019(1), article 3612535. https://doi.org/10.1155/2019/3612535

Lu, W., Qiu, H., Zhan, X., Li, T., and Lam, F. (2025). "Experimental investigation on some influencing factors of the lateral resistant behavior of wood infill walls in

traditional timber frames," *Journal of Building Engineering* 106, article 112687. https://doi.org/10.1016/j.jobe.2025.112687

LY/T 3297 (2022). "Dynamic test method for shear modulus of wood," Standardization Administration of China, Beijing, China.

Meng, X., Li, T., and Yang, Q. (2019). "Experimental study on the seismic mechanism of a full-scale traditional Chinese timber structure," *Engineering Structures* 180, 484-493. https://doi.org/10.1016/j.engstruct.2018.11.055

Meng, X., Wang, Z., Li, T., Zhang, C., Chen, J., and Yu, P. (2025, June). "Experimental and numerical investigation on the seismic performance of a traditional Chinese Song-style timber structure with roof," in: *Structures* Vol. 76, article 109019, Elsevier. https://doi.org/10.1016/j.istruc.2025.109019

Niu, Q. (2017). *Experimental Study and Theoretical Analysis on Half-Scale Model of Timber Structure in Song Dynasty*, Master's Thesis, Taiyuan University of Technology, Taiyuan, China.

Suzuki, Y., and Maeno, M. (2006). "Structural mechanism of traditional wooden frames by dynamic and static tests," *Structural Control Health Monitoring* 13, 508-522. https://doi.org/10.1002/stc.153

Wang, X., Zhang, M., Tan, Z., Liu, Y., Wei, K., Wang, X., and Lou, T. (2022). "Experimental and numerical study on the static and hysteretic behavior of a novel wood isolation device," *Journal of Building Engineering* 49, article 104061. https://doi.org/10.1016/j.jobe.2022.104061

Wu, C., Xue, J., and Song, D. (2024). "Experimental and numerical study on the mechanical performance of Dou-Gong bracket at the corner under vertical load," *International Journal of Architectural Heritage* 18(4), 526-550. https://doi.org/10.1080/15583058.2023.2169209

Wu, Y., Song, X., Gu, X., and Luo, L. (2018). "Dynamic performance of a multi-story traditional timber pagoda," *Engineering Structures* 159, 277-285. https://doi.org/10.1016/j.engstruct.2018.01.003

Wu, Y., Song, X., Ventura, C., and Lam, F. (2020). "Modeling hysteretic behavior of lateral load-resisting elements in traditional Chinese timber structures," *Journal of Structural Engineering* 146(5), article 04020062. https://doi.org/10.1061/(ASCE)ST.1943-541X.0002613

Yao, L. and Li, Y. (2023). "Simulation study on static characteristics of Qing-style 'One Bucket Three Liters' column-cap Dou-Gong bracket," *BioResources* 18(4), 6955-6970. https://doi.org/10.15376/biores.18.4.6955-6970

Article submitted: October 27, 2025; Peer review completed: January 18, 2026;
Revisions accepted: April 28, 2026; Published: April 30, 2026.
DOI: 10.15376/biores.21.2.5389-5406